nature neuroscience

SK channels and NMDA receptors form a Ca^{2+}-mediated feedback loop in dendritic spines

Thu Jennifer Ngo-Anh[1,4], Brenda L Bloodgood[2,4], Michael Lin[1], Bernardo L Sabatini[2], James Maylie[3] & John P Adelman[1]

Small-conductance Ca^{2+}-activated K^+ channels (SK channels) influence the induction of synaptic plasticity at hippocampal CA3–CA1 synapses. We find that in mice, SK channels are localized to dendritic spines, and their activity reduces the amplitude of evoked synaptic potentials in an NMDA receptor (NMDAR)-dependent manner. Using combined two-photon laser scanning microscopy and two-photon laser uncaging of glutamate, we show that SK channels regulate NMDAR-dependent Ca^{2+} influx within individual spines. SK channels are tightly coupled to synaptically activated Ca^{2+} sources, and their activity reduces the amplitude of NMDAR-dependent Ca^{2+} transients. These effects are mediated by a feedback loop within the spine head; during an excitatory postsynaptic potential (EPSP), Ca^{2+} influx opens SK channels that provide a local shunting current to reduce the EPSP and promote rapid Mg^{2+} block of the NMDAR. Thus, blocking SK channels facilitates the induction of long-term potentiation by enhancing NMDAR-dependent Ca^{2+} signals within dendritic spines.

In CA1 hippocampal neurons, apamin-sensitive SK channels modulate firing frequency by contributing to the after-hyperpolarization (AHP) that follows an action potential[1–3]. Additionally, blocking SK channels with apamin facilitates the induction of long-term potentiation (LTP) at Schaffer collateral–CA1 synapses. Apamin shifts the point of inflection between long-term depression (LTD) and long-term potentiation (LTP) such that lower stimulus frequencies[4] can generate LTP. Results from behavioral experiments parallel the effects induced by apamin in brain slices. Apamin crosses the blood-brain barrier[5], and intraperitoneal injection facilitates the acquisition of hippocampal-dependent learning tasks such as locating the hidden platform in the Morris water maze, and novel object recognition[4].

Several forms of long-term plasticity at the CA3–CA1 synapses are triggered by Ca^{2+} influx through NMDARs, and the kinetics and amplitude of evoked Ca^{2+} transients in the postsynaptic cell determine the direction and extent of synaptic plasticity. A relatively smaller and prolonged Ca^{2+} buildup results in LTD, whereas a larger, more transient increase favors LTP[6–12]. Examination of Ca^{2+} signals within CA1 dendritic spines demonstrates that synaptic stimulation results in NMDAR-mediated increases in Ca^{2+} that are limited to the spine head housing the activated synapse[13]. At resting potentials, NMDARs are largely blocked by extracellular Mg^{2+} ions[14]. The apparent affinity of Mg^{2+} for the receptor is strongly voltage-dependent, and Ca^{2+} influx is greatly accentuated by depolarization. Thus, membrane potential exerts a strong influence on spine Ca^{2+} transients, which influences downstream Ca^{2+}-dependent processes such as the induction of synaptic plasticity.

Here we show that SK channels are localized to dendritic spines and play a role in shaping synaptic responses. Apamin-sensitive SK channels are activated by synaptically evoked Ca^{2+} transients and act to reduce the magnitude of excitatory postsynaptic potentials (EPSPs) measured at the soma. This negative regulation occurs within individual spines, where SK channels respond to rapid increases in Ca^{2+} and reduce the amplitude of NMDAR-mediated Ca^{2+} transients. The effects of different Ca^{2+} buffers show that SK channels are positioned within a synaptically activated Ca^{2+} signaling microdomain and act rapidly to influence the EPSP.

RESULTS

SK channel distribution in cultured hippocampal neurons

We expressed mouse SK2 channels harboring an extracellular triple-myc epitope tag (mSK2-myc)[15] and green fluorescent protein (GFP) in dissociated, cultured neurons from area CA1 of the hippocampus. Live-cell immunostaining with a monoclonal antibody to myc (anti-myc) performed 1 week after transfection showed that virtually every spine was clearly decorated with SK2 channels (**Fig. 1**). Immunoreactivity was also present in clusters within the dendritic shafts and in the soma. Thus, exogenously expressed SK2 channels localize to dendritic spines where they are positioned along with NMDARs in the confined Ca^{2+} signaling domain of glutamatergic synapses.

Apamin increases synaptically evoked EPSPs

We recorded the effects of apamin on subthreshold EPSPs in whole-cell current-clamped CA1 neurons in acute slices from mouse

[1]Vollum Institute, Oregon Health & Science University, 3181 SW Sam Jackson Park Road, Portland, Oregon 97239, USA. [2]Department of Neurobiology, Harvard Medical School, 200 Longwood Ave., Goldenson 316, Boston, Massachusetts 02115, USA. [3]Department of Obstetrics and Gynecology, Oregon Health & Science University, 3181 SW Sam Jackson Park Road, Portland, Oregon 97239, USA. [4]These authors contributed equally to this work. Correspondence should be addressed to J.P.A. (adelman@ohsu.edu).

Published online 24 April 2005; doi:10.1038/nn1449

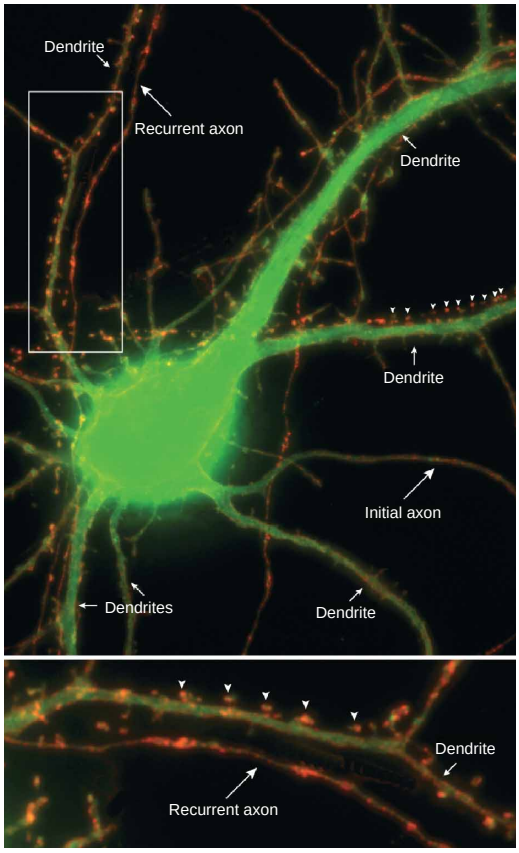

Figure 1 Live-cell immunostaining of a cultured hippocampal neuron expressing mSK2-myc (red) and cytosolic GFP (green). SK2 channel immunoreactivity can be seen in virtually every spine. Clusters of SK2 immunoreactivity were detected in the dendritic shafts and a recurrent axon. Although obscured by the intensity of the GFP fluorescence, a more homogeneous SK2 staining pattern was detected in the soma.

hippocampus. After whole-cell formation, we applied a 100-μs current pulse to the stratum radiatum, and we adjusted the stimulus strength to approximately one-third of the threshold needed to evoke an action potential, yielding EPSPs with amplitudes of 2–8 mV. Blocking NMDA receptors with AP5 (D(-)-2-amino-5-phosphono-valeric acid; 100 μM) reduced subthreshold EPSP amplitudes to an average of 76 ± 3.8% of the control, and application of AP5 with 6-cyano-7-nitroquinoxaline-2,3-dione (CNQX; 20 μM) to block α-amino-3-hydroxy-5-methyl-4-isoxazole propionic acid receptors (AMPARs) essentially eliminated the EPSPs, reducing the average amplitude to 4.7 ± 0.6% of the control ($n = 3$; data not shown). These data show that although the EPSP results primarily from activation of AMPARs, a small but measurable contribution is made by current flow through NMDARs.

To determine whether apamin-sensitive SK channels shape the synaptic potential, EPSPs were recorded every 20 s before (control solution) and after wash-in of apamin (100 nM; **Fig. 2**). In a representative cell (**Fig. 2a**,**b**), the peak EPSP, measured from the average of 20 EPSPs, increased from 3.3 mV in the control solution to 5.6 mV after apamin application. Subsequent application of AP5 (100 μM) reversed the apamin-induced increase of the EPSP amplitude; in the presence of apamin and AP5, the peak of the averaged EPSP was 2.5 mV. On average, apamin increased the amplitude of the EPSP to 173 ± 16% of the control ($P < 0.05$, $n = 5$) and subsequent co-application of AP5 reduced the EPSP amplitude to 79 ± 13% of the control (**Fig. 2c** and **Table 1**). The apamin effect was observed in every cell tested.

SK channels are the only known targets for apamin, but apamin does not reliably wash out of the slice. Therefore, the effects of D-tubocurarine (dTC; 100 μM)[16], a more reversible though less selective SK channel blocker, were also examined. In six cells tested, dTC increased the amplitude of the EPSP to 216 ± 53% ($P < 0.05$) of the control. The increase induced by dTC was largely, though not completely, reversed upon washout (154 ± 21% of the control; $P = 0.05$; **Table 1**).

The induction of long-term potentiation usually requires repetitive synaptic activation, and apamin shifts the threshold for the induction of synaptic plasticity to lower stimulus frequencies[4,17]. Therefore, we examined the effect of apamin on the summated EPSP during a synaptically evoked train of five pulses at 100 Hz. In a representative cell (**Fig. 2d**) apamin increased the average summated EPSP by 4 mV to 153% of the control. Across five cells tested, apamin

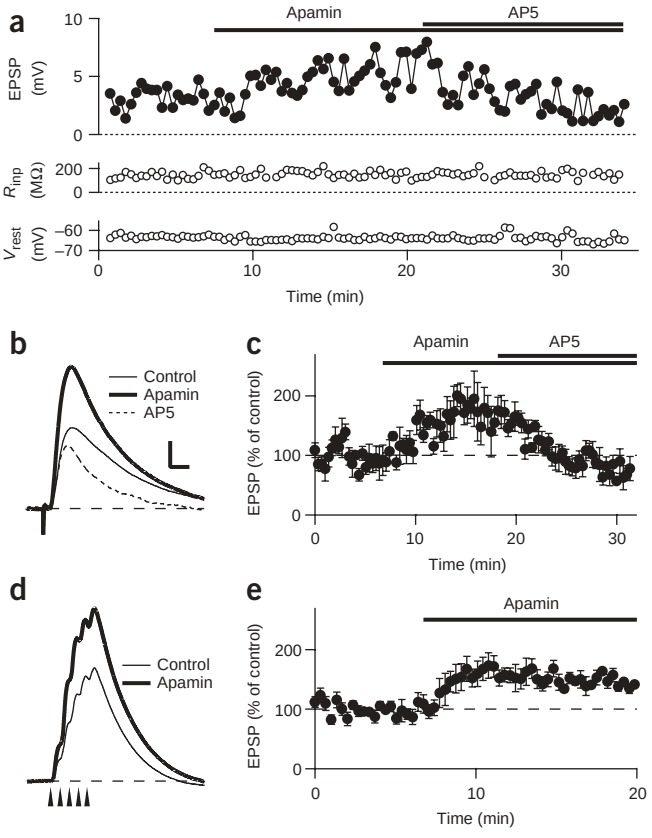

Figure 2 SK channels modulate synaptically evoked EPSPs. (**a**) Plot of EPSP amplitude (top), input resistance (middle) and membrane potential (bottom) from a representative cell during wash-in of apamin (100 nM) and apamin plus AP5 (100 μM). (**b**) Average of 20 EPSPs acquired in control conditions, in the presence of apamin or in the presence of apamin plus AP5. (**c**) Summary plot of the EPSP amplitude relative to the baseline period during wash-in of apamin and in the presence of apamin plus AP5 ($n = 5$ cells). (**d**) Average of 15 summated EPSPs under control conditions and in the presence of apamin from a representative cell. Arrowheads indicate stimulus times (five pulses at 100 Hz). (**e**) Summary plot of the effects of apamin on the summated EPSP ($n = 5$ cells). The times of drug application are indicated by the horizontal bars. Scale bar: 1 mV in **b**, 2 mV in **d**, 25 ms for **b** and **d**. Error bars are mean ± s.e.m.

Table 1 Effects of apamin on synaptically evoked EPSPs

Condition (*n*)	EPSP (mV)		Slope (V/s)		HW (ms)	Rise time (ms)
Control	3.3 ± 0.4		0.84 ± 0.13		35 ± 4	4.5 ± 0.2
Apamin	5.6 ± 0.5	(173 ± 16%)[a]	1.14 ± 0.09	(141 ± 12%)[a]	40 ± 3	5.0 ± 0.1
Apamin + AP5 (5)	2.7 ± 0.6	(79 ± 13%)	0.70 ± 0.10	(84 ± 8%)	33 ± 5	4.9 ± 0.3
Control	3.4 ± 0.5		0.72 ± 0.11		44 ± 9	6.6 ± 1.0
dTC	7.0 ± 1.2	(216 ± 53%)[a]	0.96 ± 0.09	(146 ± 23%)[a]	47 ± 6	8.7 ± 0.9
Washout (6)	5.1 ± 0.8	(154 ± 21%)	0.90 ± 0.10	(131 ± 11%)[a]	41 ± 10	6.1 ± 0.9
Control	4.1 ± 0.3		0.96 ± 0.07		40 ± 8	4.6 ± 0.6
AP5	3.2 ± 0.3	(78 ± 5%)[a]	0.76 ± 0.05	(80 ± 4%)[a]	44 ± 8	4.8 ± 0.5
AP5 + Apamin (7)	3.1 ± 0.3	(96 ± 3%)	0.71 ± 0.06	(93 ± 5%)	48 ± 8	5.9 ± 1.1
Control (0.2 mM Mg^{2+})	1.7 ± 0.2		0.62 ± 0.07		56 ± 7	7.4 ± 1.4
Apamin (6)	4.3 ± 0.2	(266 ± 29%)[a,b]	1.00 ± 0.08	(167 ± 10%)[a]	43 ± 3	6.1 ± 1.1
Control (CNQX)	1.3 ± 0.3		0.5 ± 0.2		82 ± 22	10.8 ± 3.2
Apamin (9)	4.1 ± 1.0	(320 ± 52%)[a]	0.7 ± 0.2	(171 ± 20%)[a]	105 ± 26	16.1 ± 4.5
AP5 (5)	0.3 ± 0.1	(12 ± 18%)	nd		Nd	nd
Control (5 mM BAPTA)	2.5 ± 0.6		1.55 ± 0.61		35 ± 4	5.0 ± 0.5
Apamin (6)	2.1 ± 0.5	(89 ± 3%)	1.47 ± 0.57	(104 ± 12%)	35 ± 4	4.8 ± 0.8
Control (5 mM EGTA)	3.5 ± 0.7		0.86 ± 0.12		40 ± 5	4.4 ± 0.7
Apamin (8)	6.7 ± 0.9	(214 ± 32%)[a]	1.41 ± 0.17	(170 ± 15%)[a]	35 ± 5	4.4 ± 0.3
Control (1 mM BAPTA)	5.8 ± 0.8		1.16 ± 0.12		27 ± 8	4.6 ± 0.5
Apamin (5)	7.8 ± 0.7	(140 ± 11%)[a]	1.66 ± 0.13	(147 ± 15%)[a]	27 ± 7	4.5 ± 0.5

Properties of synaptically evoked responses. Slope is defined as the maximum rate of rise of the EPSP. Rise time is defined as the time required for the EPSP to rise from 20 to 80% of the maximum amplitude. Half-width (HW) is the width of the synaptic potential measured at 50% of the maximum amplitude. Numbers in parentheses are percentage of the control for each condition.
[a]$P < 0.05$ compared with control. [b]$P < 0.05$ compared with increase in normal bath solution.

application increased the summated EPSP to 159 ± 15% of the control ($P < 0.05$; **Fig. 2e**).

NMDAR activity is required for apamin sensitivity of EPSPs

Dendritic spines are autonomous Ca^{2+} signaling compartments highly specialized for the rapid large-amplitude Ca^{2+} fluctuations that underlie synaptic plasticity[13]. The results presented above suggest that the effects of apamin on the amplitude of the EPSP are due to regulation of NMDARs in response to synaptically evoked increases in Ca^{2+}. Therefore, applying NMDAR blockers such as AP5 before apamin should occlude apamin's effects. Indeed, blocking NMDARs with AP5 reduced the EPSP to 78 ± 5% of the control ($P < 0.05$), and subsequent application of AP5 with apamin had no effect on the EPSP amplitude (96 ± 3% of the value recorded with AP5, $n = 7$; **Fig. 3a,b** and **Table 1**).

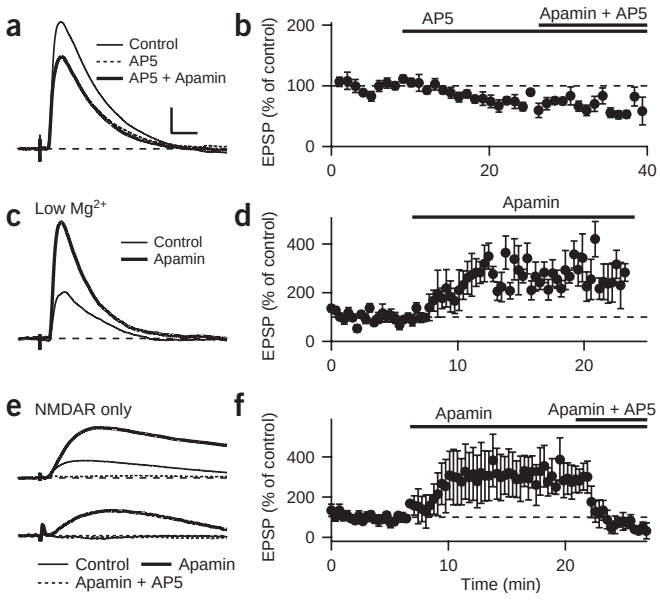

Figure 3 Apamin-induced EPSP increases require NMDAR activity. (**a**) Average of 25 EPSPs in control conditions, in the presence of AP5, or in the presence of AP5 plus apamin from a representative cell. (**b**) Summary plot of the effects of AP5 or AP5 plus apamin application on EPSP peaks ($n = 7$ cells). (**c**) Average EPSPs in solutions containing 0.2 mM external Mg^{2+} or 0.2 mM Mg^{2+} plus apamin. (**d**) Summary plot of the effects of apamin application on EPSP peaks in the presence of low external [Mg^{2+}] ($n = 6$). (**e**) Average evoked EPSPs recorded in the presence of CNQX and no Mg^{2+} (control) and with the additional application of apamin or AP5 plus apamin. Examples are shown in which the NMDAR-dependent EPSP was clearly visible (top) or not detectable (bottom) before apamin application. (**f**) Summary plot of the effects of apamin and apamin plus AP5 on the peak of the isolated NMDAR-mediated EPSP ($n = 5$). The times of drug application are indicated by the horizontal bars. Scale bar: 1 mV for **a**,**c**, 0.5 mV for **e**, and 25 ms for **a**,**c**,**e**. Error bars are mean ± s.e.m.

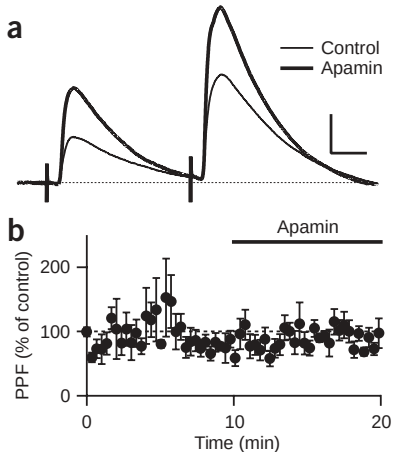

Figure 4 Apamin has no effect on paired pulse facilitation. (**a**) Synaptically evoked EPSP pairs (100-ms inter-pulse interval) under control conditions and in the presence of apamin from a representative cell. Scale bar: 1 mV, 25 ms. (**b**) Summary plot of PPF relative to control values during application of apamin as indicated by the horizontal bar ($n = 6$ cells). Error bars are mean ± s.e.m.

SK channels are activated by changes in intracellular Ca^{2+}, suggesting that augmenting synaptically evoked Ca^{2+} influx should increase SK channel activation and amplify the effect of apamin on the EPSP. As ~80% of the Ca^{2+} transient in dendritic spines is due to Ca^{2+} influx through NMDARs (see below), reducing Mg^{2+} block of NMDARs by lowering the external Mg^{2+} concentration ($[Mg^{2+}]$) to 0.2 mM should result in larger synaptically evoked Ca^{2+} influx. Under these conditions, apamin application increased the EPSP to 266 ± 29% of the control ($P < 0.05$, $n = 6$), which was larger than the apamin-induced increase when external $[Mg^{2+}]$ was 1 mM ($P < 0.05$; **Fig. 3c**,**d** and **Table 1**). Preincubation with AP5 occluded the apamin-induced change in the EPSP in the presence of 0.2 mM Mg^{2+} (data not shown).

We examined the effects of apamin on the isolated NMDAR component of the response by recording EPSPs while blocking AMPARs (**Fig. 3e**,**f**). In initial experiments, setting the stimulus strength in control conditions to one-third of threshold compromised the ability of the stimulus to reliably elicit an EPSP after addition of AMPAR blockers, although subsequent application of apamin showed an EPSP that was eliminated by AP5 (**Fig. 3e**). To enhance the NMDAR component, the stimulus strength was increased in AMPAR blockers to yield a detectable EPSP. Apamin increased the NMDAR-mediated EPSP to 320 ± 52% of that in the presence of CNQX ($P < 0.05$, $n = 9$), and subsequent application of AP5 to five of the cells essentially eliminated the EPSP (0.3 ± 0.1 of the control; **Fig. 3e**,**f** and **Table 1**).

Figure 5 Single synapse responses and NMDAR-dependent spine Ca^{2+} signals evoked with two-photon uncaging of glutamate. (**a**) Image of an apical spiny dendrite of a CA1 hippocampal pyramidal neuron collected with two-photon laser scanning microscopy (left). Fluorescence from the red Alexa Fluor 594 channel is shown. Simultaneously recorded green (Fluo-5F) and red (Alexa Fluor 594) fluorescence (right) were collected in line scans that intersect the spine head and neighboring dendrite indicated by the dashed line (left). The current was evoked by a 0.5-ms, 720-nm glutamate uncaging pulse directed at the spine indicated by the arrowhead. Increases in green fluorescence, indicative of elevations in intracellular Ca^{2+}, were limited to the stimulated spine head. Scale bar: 1 μm (left), 25 ms (right). (**b**) For the spine depicted in **a**, uncaging parameters were set to evoked a ~15-pA uEPSC (top). After switching to current-clamp mode and leaving the uncaging pulse unchanged, the uEPSP (middle) and fluorescence transient ($\Delta G/R_{syn}$, bottom) were recorded. (**c**) Representative uEPSC (top), uEPSP (middle) and accompanying Ca^{2+} transient (bottom) recorded in the presence of NMDAR blockers (20 μM CPP and 40 μM MK801). Each trace is the average of ten trials. Scale bar: 6 pA (top), 0.45 mV (middle), 3% *G/R* (bottom), and 25 ms.

Apamin increases EPSPs by a postsynaptic mechanism

The model presented above suggests that apamin acts postsynaptically, but bath application of apamin may have both pre- and postsynaptic effects. Paired-pulse facilitation (PPF), defined as the ratio of the amplitude of the second EPSP to that of the first after a closely delivered pair of stimuli, is a sensitive assay of presynaptic changes in glutamate release probability[18]. When we applied paired-pulse stimulations separated by 100 ms, apamin application increased the peaks of the EPSPs without altering PPF (2.47 ± 0.47 in the control, 2.07 ± 0.19 in the presence of apamin, $n = 6$; **Fig. 4a**,**b**). This result is consistent with a postsynaptic site of action of apamin.

Apamin increases synaptically evoked spine Ca^{2+} influx

Taken together, our results suggest that SK channels reside in the dendritic spine head, close to synaptically evoked Ca^{2+} sources. If opening SK channels imposes a repolarization that favors Mg^{2+} block of NMDARs, then blocking SK channels with apamin should increase the amplitude and prolong the duration of NMDAR-mediated Ca^{2+} influx. To test this hypothesis, spine Ca^{2+} transients were examined with two-photon laser scanning microscopy while the synapse on the visualized spine was stimulated with two-photon laser uncaging of 4-methoxy-7-nitroindolinyl (MNI)-glutamate (**Fig. 5**; ref. 19). Two-photon laser uncaging allows the selective stimulation of the synapse on any visualized spine, and because of the brief and focal release of glutamate, it can be used to accurately mimic the time course of innate synaptic events in hippocampal pyramidal neurons[20]. Furthermore, two-photon laser uncaging is advantageous over electrical stimulation of axonal fibers because it allows the true stimulation of a single synapse on the cell, avoiding stimulation of multiple synapses that may lead to secondary activation of active conductances, altering the EPSP amplitude and time course. Lastly, by bypassing the presynaptic terminal, failures of synaptic transmission are avoided and trial-to-trial variability is reduced, allowing population comparison of synaptic responses in control conditions and in the presence of apamin.

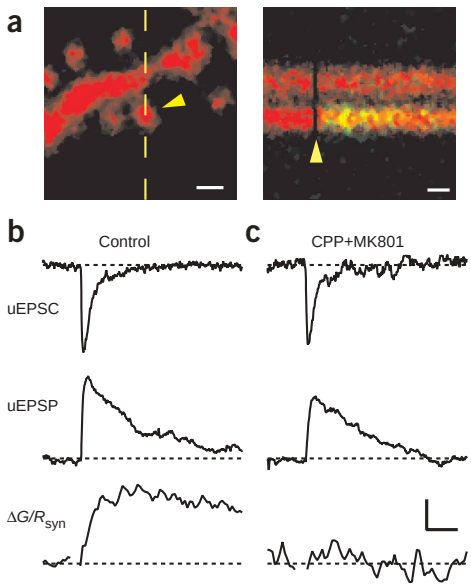

Table 2 Properties of single-spine uncaging–evoked responses.

	uEPSC			uEPSP		
Condition (*n*)	Amplitude (pA)	Rise time (ms)	HW (ms)	Amplitude (mV)	Rise time (ms)	HW (ms)
Control (24)	−15.1 ± 0.5 (100 ± 3%)	1.1 ± 0.1 (100 ± 9%)	6.7 ± 0.5 (100 ± 7%)	0.92 ± 0.09 (100 ± 10%)	2.8 ± 0.3 (100 ± 11%)	30 ± 3 (100 ± 10%)
Apamin (25)	−14.7 ± 0.5 (97 ± 3%)	1.4 ± 0.1 (127 ± 13%)	8.0 ± 0.7 (119 ± 10%)	1.00 ± 0.07 (109 ± 8%)	3.4 ± 0.3 (121 ± 11%)	45 ± 4[a] (150 ± 13%)
CPP + MK801 (21)	−14.7 ± 0.8 (97 ± 5%)	1.3 ± 0.1 (118 ± 13%)	7.6 ± 0.7 (113 ± 10%)	1.02 ± 0.11 (111 ± 12%)	3.3 ± 0.3 (118 ± 9%)	37 ± 3 (123 ± 10%)
Apamin + CPP + MK801 (22)	−15.0 ± 0.8 (99 ± 5%)	1.3 ± 0.1 (118 ± 13%)	8.5 ± 0.6 (126 ± 9%)	1.08 ± 0.10 (117 ± 11%)	2.5 ± 0.2 (89 ± 7%)	30 ± 3 (100 ± 10%)

Rise time is defined as the time required for the EPSP or EPSC to rise from 20 to 80% of the maximum amplitude.HW is the width of the synaptic current or potential measured at 50% of the maximum amplitude. In parentheses for each condition are mean ± s.e.m. expressed as a percentage of the mean value in the 'control' condition.
[a]$P < 0.05$ by ANOVA, comparing measurements in control conditions with measurements in the presence of apamin; or comparing measurements in the presence of CPP plus MK801 with measurements in the presence of apamin plus CPP plus MK801.

CA1 pyramidal neurons were filled with the Ca^{2+}-sensitive fluorophore Fluo-5F (300 μM) to record Ca^{2+} transients and with the Ca^{2+}-independent fluorophore Alexa Fluor 594 (10 μM) to visualize spines and dendrites. Both fluorophores are efficiently two-photon excited by 810-nm laser light, with Fluo-5F emitting in the green (500–560 nm) and Alexa Fluor 594 emitting in the red (585–630 nm). Under these conditions, changes in green fluorescence relative to resting red fluorescence ($\Delta G/R$) are linearly proportional to increases in intracellular [Ca^{2+}] after subthreshold synaptic stimulation[13].

We selected spines within the proximal (<150 μm) apical dendrite for analysis. Cells were initially held in voltage clamp, and we set the uncaging laser pulse duration and amplitude to evoke a ~15-pA synaptic current (uEPSC; **Fig. 5b**, top, and **Table 2**). The amplifier was subsequently switched to current-clamp mode, and the uncaging-evoked EPSP (uEPSP) and synaptically evoked Ca^{2+} transient were monitored with the same uncaging parameters (**Fig. 5b**, middle, bottom). The fluorescence transient accompanying the uEPSP was recorded in line scan mode (500 Hz) from the stimulated spine head ($\Delta G/R_{syn}$) and the neighboring parent dendrite. In basal conditions, the uEPSP had an amplitude of 0.92 ± 0.09 mV, a 20–80% rise time (the time required for the EPSP to rise from 20 to 80% of its maximum amplitude) of 2.8 ± 0.3 ms and a half-width (the width of the synaptic potential measured at 50% of the maximum amplitude) of 30 ± 3 ms (properties of the uEPSC and uEPSP are summarized in **Table 2**). The uEPSP was accompanied by an increase in spine Ca^{2+} levels ($\Delta G/R_{syn}$ = 7.1 ± 0.8%) that rose quickly (20–80% rise time = 13 ± 2.0 ms) and was limited to the stimulated spine. After stimulation, Ca^{2+} remains elevated in the spine head because of the slow clearance of Ca^{2+} from the spine in the presence of Ca^{2+} indicator[13].

To confirm that the evoked Ca^{2+} influx was due to activation of NMDARs, the same experiments were repeated in the presence of the NMDAR antagonists 2-carboxypiperazin-4-yl-propyl-1-1 phosphonic acid (CPP, 20 μM) and MK801 (40 μM; **Fig. 5c**). In these conditions, the uEPSC and uEPSP were unchanged from control conditions (**Table 2**) whereas the amplitude of synaptically evoked Ca^{2+} transients was reduced to 1.3 ± 0.3% $\Delta G/R_{syn}$ (17% of the control levels). Thus, Ca^{2+} influx through NMDARs contributes the majority of the Ca^{2+} evoked by uEPSPs.

The effect of activation of SK channels on the amplitude of the Ca^{2+} transients within individual spine heads that contain active synapses was examined in a population of cells exposed to apamin (100 nM). The properties of the uEPSC were unaffected, and the uEPSP was slightly increased (**Fig. 6** and **Table 2**). The smaller effect on synaptic potentials seen here is likely due to the reduced SK channel activation in

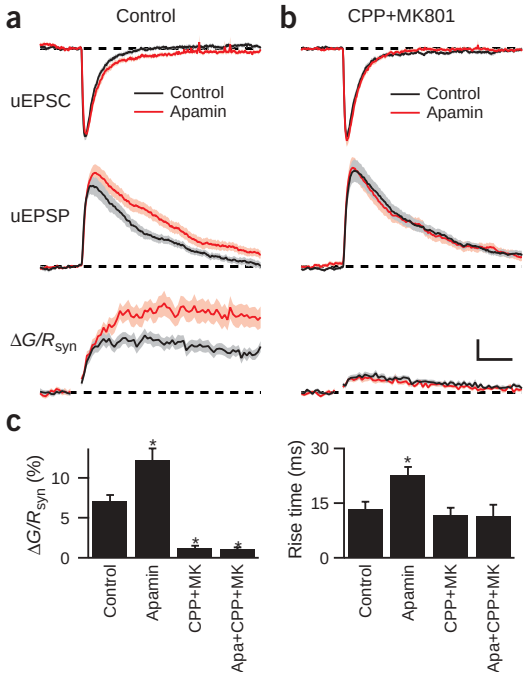

Figure 6 Blocking SK channels with apamin increases NMDAR-mediated spine Ca^{2+} transients. (**a**) Average uEPSC, uEPSP and $\Delta G/R_{syn}$ under control conditions and in the presence of apamin (n = 24 and 25 spines, respectively). (**b**) Average uEPSC (top), uEPSP (middle) and $\Delta G/R_{syn}$ (bottom) in the presence of NMDAR blockers (black) and NMDAR blockers + apamin (red; n = 21 and 22 spines, respectively). Scale bar: 6 pA (top), 0.45 mV (middle) and 6% G/R (bottom), and 25 ms for **a**,**b**. The shaded region shows the mean ± s.e.m. for each average trace. (**c**) Comparison of the Ca^{2+} transient amplitude and rise time each condition. *, $P < 0.05$ compared with control.

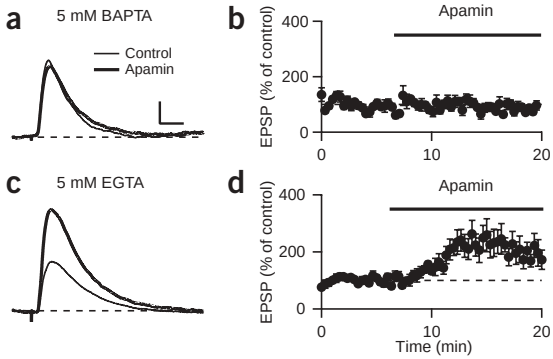

Figure 7 Effects of BAPTA and EGTA on the apamin-induced increase of the EPSP. (**a**,**c**) Synaptically evoked EPSPs were recorded in control conditions or in the presence of apamin with either 5 mM BAPTA or 5 mM EGTA in the patch pipette as indicated. (**b**,**d**) Summary plots of the effects of apamin on EPSP peaks for intracellular solutions containing 5 mM BAPTA (**b**; $n = 10$ cells) or 5 mM EGTA (**d**; $n = 8$ cells). The time period of apamin application is indicated by the bars. Scale bar: 1 mV and 25 ms. Error bars are mean ± s.e.m.

the presence of the BAPTA-based indicator Fluo-5F and the large variability of single-synapse evoked potentials (coefficient of variation of ~50%). The amplitude and the rising phase of uEPSP-evoked Ca^{2+} influx in the presence of apamin were increased to 12.2 ± 1.5% $\Delta G/R_{syn}$ and 23 ± 2 ms, or 172% and 169% of the control, respectively. The effects of SK channel blockage require active NMDARs, because in the presence of CPP plus MK801, the uEPSC, uEPSP, and $\Delta G/R_{syn}$ were identical in control conditions and in the presence of apamin (**Fig. 6b**). Thus, after activation of a single synapse, SK channels act within the active spine to reduce the amplitude of NMDAR-mediated Ca^{2+} transients.

SK channels and Ca^{2+} sources form a microdomain

Our results indicated that SK channels are located on the spine and regulate Ca^{2+} influx into the active spine head in response to synaptically activated Ca^{2+} sources. To estimate the distance between SK channels and the Ca^{2+} source that activates them, synaptically evoked EPSPs were recorded in the presence of BAPTA, a rapid Ca^{2+} chelator, or EGTA, a slower Ca^{2+} chelator, in the internal solution. When the neuron was dialyzed with 5 mM BAPTA, the effects of apamin on the EPSP amplitude were occluded (89 ± 3% of the control, $n = 6$; **Fig. 7a**,**b** and **Table 1**). In contrast, when 5 mM EGTA was included in the pipette solution, application of apamin increased the EPSP to 214 ± 32% of the control ($P < 0.05$, $n = 8$; **Fig. 7c**,**d** and **Table 1**), which was not different from the increase induced by apamin in the control internal solution. Additionally, with 1 mM BAPTA in the pipette solution, the apamin-mediated increases of the EPSP were 140 ± 11% of the control ($P < 0.05$, $n = 5$; **Table 1**). These results further support a postsynaptic action by apamin and, notably, are consistent with a close spatial coupling between SK channels and synaptically activated Ca^{2+} sources within individual spine heads.

DISCUSSION

The central finding of this work is that in dendritic spines of CA1 neurons, Ca^{2+} entry after synaptic activation opens SK channels that act to limit the amplitude of synaptic potentials and reduce Ca^{2+} influx through NMDARs. As described below, this feedback loop is engaged by the activity of a single synapse and regulates NMDAR-evoked Ca^{2+} influx within the active spine head. As NMDAR-mediated Ca^{2+} is quantitatively critical to the processes underlying the induction of synaptic plasticity[6–12], this feedback loop likely accounts for the effects of apamin on the threshold for LTP induction. Furthermore, our results suggest that SK channel modulation offers a powerful mechanism to fine-tune the induction of synaptic plasticity.

Effects of apamin of synaptic responses

Blocking SK channels with apamin increases the synaptically evoked EPSP amplitude. This effect is prevented by pretreatment with NMDAR blockers and is still present when the NMDAR component of the EPSP is isolated. Thus, NMDARs are necessary and sufficient for the effects of apamin on the EPSP, and apamin increases synaptic potentials by enhancing the normally small contribution of the NMDAR to the EPSP. The large effect that apamin has on NMDAR activation is particularly evident when the isolated NMDAR component of the EPSP is examined. Despite the small, or in several cells, undetectable, NMDAR-mediated response to synaptic stimulation, apamin application demonstrated a prominent AP5-sensitive EPSP. As NMDARs are responsible for the majority of the Ca^{2+} influx into the spine head evoked by uncaging, their increased activation in the presence of apamin boosts spine head Ca^{2+} transients by 72%. The effects of apamin on spine Ca^{2+} transients were, by necessity, monitored in cells loaded with Ca^{2+} indicators that reduce the amplitude of evoked Ca^{2+} transients and subsequent activation of SK channels. Therefore, apamin application is likely to increase synaptically evoked spine Ca^{2+} transients even more robustly in neurons free of BAPTA-based Ca^{2+} buffers.

Apamin also increases the initial slope of the EPSP to a similar extent that it increases the amplitude (**Table 1**). The initial slope was measured as the maximum rate of rise of the EPSP, which usually occurs between 10 and 20% of the rise time (~2 ms into the EPSP). The initial slope was increased for both the rapidly rising, mixed AMPAR- and NMDAR-mediated EPSP, and for the slower, isolated NMDAR-mediated EPSP, which had 20–80% rise times of 5.0 ± 0.1 ms and 16.1 ± 4.5 ms, respectively. Is the effect of apamin on the rate of rise of the EPSP compatible with the slow opening of NMDARs? The macroscopic kinetics of the synaptically evoked NMDAR-mediated component of the EPSP, which reaches a peak in about 20 ms (refs. 21,22), has been attributed to the intrinsic gating kinetics of the channel[23,24]. Complementary single-channel records show that gating is complicated, but heterologously expressed NMDARs are activated with 10–90% rise times of ~7–11 ms (refs. 25,26). The predominant component of Mg^{2+} unblocking of NMDARs is very fast, occurring in ~100 μs (ref. 27) and is not rate-limiting. Taken together, these data suggest that at least a small number of NMDARs open early in the response and contribute to the rising phase and peak of the EPSP. These early-opening channels may also provide the source of Ca^{2+} that rapidly activates apamin-sensitive SK channels.

Regulation of synaptic responses by SK channels

Our data indicate that SK channels are located near glutamatergic synapses in dendritic spines. We demonstrate that exogenously expressed SK2 channels are targeted to spine heads and that activation of a single synapse engages SK channels to regulate NMDAR-dependent Ca^{2+} influx within the active spine head. What synaptically evoked Ca^{2+} sources open SK channels? Our results demonstrate that ~80% of the spine head Ca^{2+} influx is contributed by NMDARs, and the remaining 20% is likely to reflect activation of voltage-sensitive Ca^{2+} channels, which in spines of hippocampal pyramidal neurons are

R-type[28,29]. Thus, rapid Ca^{2+} influx through NMDARs that open in the early portion of the EPSP (see above), along with a possible contribution from voltage-sensitive Ca^{2+} channels, is likely to provide the signal that activates SK channels.

The close association between synaptically activated Ca^{2+} sources and SK channels is supported by results showing that 5 mM BAPTA, a rapid Ca^{2+} chelator, is capable of intercepting the Ca^{2+} ions before they encounter SK channels, whereas the slower Ca^{2+} chelator EGTA, at the same concentration, does not block the effect. The characteristic distance for the diffusion of Ca^{2+} in three dimensions before capture by a buffer can be approximated by $\sqrt{6D_{Ca}/k_{on}[buffer]}$, where D_{Ca} is the diffusion coefficient of Ca^{2+}, k_{on} is the apparent forward rate constant of Ca^{2+} binding to the buffer and [buffer] is the free buffer concentration. Using a k_{on} of 4×10^8 $M^{-1}s^{-1}$ for BAPTA and a D_{Ca} of 220 μm^2 s^{-1} (ref. 30), Ca^{2+} will diffuse a characteristic distance of 26 nm before capture by 5 mM BAPTA and 58 nm before capture by 1 mM BAPTA. Therefore, the distance between the two populations of channels may be estimated at ~25–50 nm, and Ca^{2+} ions will encounter an SK channel within ~2 μs of entering the spine.

As subthreshold synaptic stimulation increases average Ca^{2+} levels within the spine head to approximately 700 nM (ref. 13), activated Ca^{2+} sources are likely to locally provide a saturating concentration (>3 μM) of Ca^{2+} to the SK channels, so that the intrinsic gating kinetics of the SK channels will influence the EPSP. Rapid application of saturating concentrations of Ca^{2+} to heterologously expressed SK channels shows that activation time constants can be <5 ms (ref. 31; unpublished results, J.M., J.P.A.), consistent with their influence on the initial slope of the EPSP. The coupling between single L-type Ca^{2+} channels and SK channels on the soma of CA1 neurons has been examined earlier[32,33]; latencies as short as 0.9 ms were demonstrated between the opening of L-type channels and SK channels, consistent with a separation of ~100 nm[34].

Our results are consistent with previous demonstrations of coupling between NMDARs and Ca^{2+}-activated K^+ channels on cultured hippocampal neurons. It has been shown previously that application of NMDA to cultured postnatal rat hippocampal neurons evoked a Ca^{2+}-activated K^+ current that was partially inhibited by dTC but was not blocked by apamin[35]. In a more recent study, NMDA was applied to the soma of cultured hippocampal neurons, and activation of an SK current was observed in approximately half of the cells.[36] That study also showed that the muscarine-sensitive, slowly activating Ca^{2+}-activated K^+ current was sometimes activated by NMDA application, but coupling to large-conductance Ca^{2+}-activated channels (BK channels) was not observed[36], as has been reported for olfactory neurons[37]. In dopamine neurons, NMDA receptor activation may decrease an associated SK current[38].

SK2 channels are of the subtype which is likely responsible for the apamin-induced effects on EPSPs, Ca^{2+} transients and synaptic plasticity. A recent study using SK knockout mice showed that SK2 channels account for the apamin-sensitive currents in CA1 neurons[39]. Consistent with this, we demonstrate that immunohistochemistry of SK2-transfected CA1 neuronal cultures detects SK2 channels in virtually every spine. In addition, SK2 channels are seen in within the dendritic shafts, where SK channel activation affects plateau potentials and the spread of dendritic Ca^{2+} spikes by influencing voltage-gated Ca^{2+} channels[40]. SK2 immunoreactivity is also observed throughout the soma, and this population may mediate the apamin-induced increase of CA1 excitability[4,34,41]. Therefore, separate populations of SK2 channels in CA1 neurons occupy discrete subcellular locales where they couple with different Ca^{2+} sources to serve distinct physiological roles.

METHODS

Cell culture and transfection. Primary cultures were prepared from the CA1 area of hippocampi of P1–2 mice as described previously[42]. Briefly, CA1 area from newborn mice were dissociated by papain treatment and trituration and plated on a bed of astrocytes at a density of ~7,100 cells cm^{-2}. Neurons were cultured in MEM and supplemented with 5% horse serum. After 7–14 d in culture, cells were transfected with Lipofectamine2000 (Invitrogen). Immunocytochemistry was performed 5–7 d after transfection. At that time, the neurons had branching dendritic arbors and well developed spines.

Immunocytochemistry. To detect triple-myc–labeled mSK2 protein on the cell surface, live cells were incubated with anti-myc mouse monoclonal antibody (Invitrogen) for 1 h (37 °C, 5% CO_2), washed, fixed, and permeabilized in 4% paraformaldehyde/4% sucrose in PBS for 30 min at room temperature (22–24 °C) and washed again. Neurons were pre-incubated in blocking solution (5% normal goat serum/1% BSA) for 30 min at room temperature, and then incubated for 1 h in Cy3-conjugated secondary antibody (Jackson ImmunoResearch). Samples were mounted with Antifade mounting medium before visualization. Imaging was performed using a Leica DM-RXA microscope equipped with Zeiss Plan Neofluor 40×/NA1.4 and 63×/NA1.25 oil immersion objective lenses and a Princeton Instruments Micromax CCD camera. Images were acquired with MetaMorph acquisition and analysis software.

Slice preparation. All procedures were done in accordance with the guidelines of the Animal Care Committees of the Oregon Health & Science University and Harvard University. Hippocampal slices were prepared from C57BL/6J mice from postnatal day 15–18 for imaging-uncaging experiments and from postnatal week 4–6 for electrophysiology experiments. Animals were anesthetized by intraperitoneal injection with either a ketamine-xylocaine cocktail or isofluorane, and decapitated. The cerebral hemispheres were quickly removed and placed into cold artificial cerebrospinal fluid (ACSF) and equilibrated with 95%O_2/5%CO_2. Hippocampi were removed, placed onto an agar block, and transferred into a slicing chamber containing sucrose-ACSF or choline-ACSF. Transverse hippocampal slices (300–375 μm) were cut with a Leica VT1000s and transferred into a holding chamber containing regular ACSF (in mM: 125 NaCl, 2.5 KCl, 21.4 $NaHCO_3$, 1.25 NaH_2PO_4, 2.0 $CaCl_2$, 1.0 $MgCl_2$, 11.1 glucose) and equilibrated with 95%O_2/5%CO_2. Slices were incubated at 35 °C for 30–45 min and then for synaptically evoked responses were allowed to recover at room temperature (22–24 °C) for ≥1.5 hrs before recordings were performed.

Electrophysiology. For synaptically evoked recordings, CA1 pyramidal cells were visualized with infrared–differential interference contrast optics (Zeiss Axioskop 2FS) and a CCD camera (Sony). Whole-cell patch-clamp recordings were obtained from CA1 pyramidal cells using an Axopatch 200A amplifier (Axon Instruments), digitized using an ITC-16 analog-to-digital converter (InstruTech) and transferred to a computer using Pulse software (Heka Elektronik). Patch pipettes (open pipette resistance, 2.5–3.5 MΩ), if not otherwise noted, were filled with a solution containing (in mM) 140 $KMeSO_4$, 8 NaCl, 1 $MgCl_2$, 10 HEPES, 5 MgATP, 0.05 EGTA(pH 7.3). EPSPs were recorded in whole-cell current-clamp mode. A bipolar tungsten electrode (FHC) was used to stimulate presynaptic axons in stratum radiatum. Picrotoxin (0.1 mM) was added in most experiments to reduce GABAergic contributions. The input resistance was determined from a ~7-pA hyperpolarizing current injection pulse given 800 ms after each synaptically evoked EPSP. Subthreshold EPSPs were elicited by 100-μs current injections that were approximately one-third of the stimulus required for evoking an action potential. In some experiments, the magnitude of the apamin-induced increase of the EPSP elicited action potentials. Under these conditions, the stimulus strength was reduced to approximately one-quarter of threshold. Recordings were made using an Axon 200A amplifier (Axon Instruments) interfaced to a Macintosh G4 with an ITC-16 computer interface (Instrutech Corp). Data were filtered at 5 kHz and collected at a sample frequency of 20 kHz using Pulse (Heka Elektronik). All recordings used cells with a resting membrane potential less than −60mV that did not change by more than 2 mV during an experiment and with a stable input resistance that did not change by more than 5%.

Data analysis. Data were analyzed using IGOR (WaveMetrics). The slope of the rising phase of the EPSP was determined from its first derivative and taken as

the maximum value during the first half of the rising phase. Data are expressed as mean ± s.e.m. Paired *t*-tests or ANOVA was used to determine significance; $P < 0.05$ was considered significant.

Pharmacology. Apamin (Calbiochem), DL-AP5 (Tocris Cookson), CPP (Tocris Cookson), and MK801 (Tocris Cookson) were dissolved in distilled water, and CNQX, NBQX, and Picrotoxin (Tocris Cookson) in ethanol to produce stock solutions (1,000× concentrated) and added to the external medium.

Two-photon uncaging and imaging. Combined two-photon uncaging of MNI-glutamate and two-photon intracellular Ca^{2+} imaging was performed using a modified, custom two-photon laser scanning microscope[43] that is described fully elsewhere[19]. Briefly, the outputs of two Ti: Sapphire lasers (Mira/Verdi, Coherent) were independently modulated with Pockels cells (350–80 and 350–50, Conoptics) and combined using polarizing optics. Glutamate was uncaged using 0.2–0.6 ms pulses of 720 nm light, and Alexa Fluor 594 and Fluo-5F were excited with 810 nm light. Fluorescence was collected in line scan mode (500 Hz) with a brief interruption (2 ms) during which the scanning mirrors were redirected to the selected spine and the uncaging pulse was triggered. Fluorescence transients were quantified as increases in green (Fluo-5F) fluorescence from baseline divided by resting red (Alexa Fluor 594) fluorescence. This method provides quantification that is insensitive to small changes in resting Ca^{2+} and independent of spine volume[13]. In our recording conditions, $\Delta G/R$ is linearly proportional to $\Delta[Ca^{2+}]$ to within ~20% (ref. 13). Off-line data analysis was performed using custom software written in Igor Pro (Wavemetrics) and MATLAB.

MNI-glutamate was included in the bath at 5 mM. Cells were filled with 300 μM Fluo-5F to report intracellular Ca^{2+} transients and 10 μM Alexa Fluor-594 to image neuronal morphology. Neurons were allowed to fill for 10–20 min before beginning Ca^{2+} imaging. Spines on secondary and tertiary dendrites within 150 μm of the soma were selected for analysis. uEPSCs and uEPSPs were monitored with an Axopatch 200B and were filtered at 2 kHz and sampled at 10 kHz.

ACKNOWLEDGMENTS

We thank T. Tzounopoulos and C. Jahr for helpful discussions. We also thank G. Banker and S. Kaech-Petrie for assistance with hippocampal cultures. This work was supported by National Institutes of Health grants to J.M. and J.P.A., and by grants to B.L.S. from the Whitaker Foundation and the Searle Scholar's program.

COMPETING INTERESTS STATEMENT

The authors declare that they have no competing financial interests.

Received 11 March; accepted 29 March 2005
Published online at http://www.nature.com/natureneuroscience/

1. Zhang, L. & McBain, C.J. Potassium conductances underlying repolarization and afterhyperpolarization in rat CA1 hippocampal interneurons. *J. Physiol. (Lond.)* **488**, 661–672 (1995).
2. Sah, P. & Mclachlan, E.M. Ca^{2+}-activated K^+ currents underlying the afterhyperpolarization in guinea pig vagal neurons: a role for Ca^{2+}-activated Ca^{2+} release. *Neuron* **7**, 257–264 (1991).
3. Lorenzon, N.M. & Foehring, R.C. Relationship between repetitive firing and afterhyperpolarizations in human neocortical neurons. *J. Neurophysiol.* **67**, 350–363 (1992).
4. Stackman, R.W. *et al.* Small conductance Ca^{2+}-activated K^+ channels modulate synaptic plasticity and memory encoding. *J. Neurosci.* **22**, 10163–10171 (2002).
5. Habermann, E. Apamin. *Pharmacol. Ther.* **25**, 255–270 (1984).
6. Lisman, J. A mechanism for the Hebb and the anti-Hebb processes underlying learning and memory. *Proc. Natl. Acad. Sci. USA* **86**, 9574–9578 (1989).
7. Mulkey, R.M. & Malenka, R.C. Mechanisms underlying induction of homosynaptic long-term depression in area CA1 of the hippocampus. *Neuron* **9**, 967–975 (1992).
8. Dudek, S.M. & Bear, M.F. Homosynaptic long-term depression in area CA1 of hippocampus and effects of N-methyl-d-aspartate receptor blockade. *Proc. Natl. Acad. Sci. USA* **89**, 4363–4367 (1992).
9. Artola, A. & Singer, W. Long-term depression of excitatory synaptic transmission and its relationship to long-term potentiation. *Trends Neurosci.* **16**, 480–487 (1993).
10. Bliss, T.V. & Collingridge, G.L. A synaptic model of memory long-term potentiation in the hippocampus. *Nature* **361**, 31–39 (1993).
11. Cummings, J.A., Mulkey, R.M., Nicoll, R.A. & Malenka, R.C. Ca^{2+} signaling requirements for long term depression in the hippocampus. *Neuron* **16**, 825–833 (1996).
12. Yang, S.N., Tang, Y.G. & Zucker, R.S. Selective induction of LTP and LTD by postsynaptic $[Ca^{2+}]_i$ elevation. *J. Neurophysiol.* **81**, 781–787 (1999).
13. Sabatini, B.L., Oertner, T.G. & Svoboda, K. The life cycle of Ca^{2+} ions in dendritic spines. *Neuron* **33**, 439–452 (2002).
14. Mayer, M.L., Westbrook, G.L. & Guthrie, P.B. Voltage-dependent block by Mg^{2+} of NMDA responses in spinal cord neurones. *Nature* **309**, 261–263 (1984).
15. Lee, W.S., Ngo-Anh, T.J., Bruening-Wright, A., Maylie, J. & Adelman, J.P. Small conductance Ca^{2+}-activated K^+ channels and calmodulin: cell surface expression and gating. *J. Biol. Chem.* **278**, 25940–25946 (2003).
16. Ishii, T.M., Maylie, J. & Adelman, J.P. Determinants of apamin and D-tubocurarine block in SK potassium channels. *J. Biol. Chem.* **272**, 23195–23200 (1997).
17. Behnisch, T. & Reymann, K.G. Inhibition of apamin-sensitive calcium dependent potassium channels facilitate the induction of long-term potentiation in the CA1 region of rat hippocampus *in vitro*. *Neurosci. Lett.* **253**, 91–94 (1998).
18. Katz, B. & Miledi, R. The role of calcium in neuromuscular facilitation. *J. Physiol. (Lond.)* **195**, 481–492 (1968).
19. Carter, A.G. & Sabatini, B.L. State-dependent calcium signaling in dendritic spines of striatal medium spiny neurons. *Neuron* **44**, 483–493 (2004).
20. Matsuzaki, M. *et al.* Dendritic spine geometry is critical for AMPA receptor expression in hippocampal CA1 pyramidal neurons. *Nat. Neurosci.* **4**, 1086–1092 (2001).
21. Bekkers, J.M. & Stevens, C.F. NMDA and non-NMDA receptors are co-localized at individual excitatory synapses in cultured rat hippocampus. *Nature* **341**, 230–233 (1989).
22. Hestrin, S., Nicoll, R.A., Perkel, D.J. & Sah, P. Analysis of excitatory synaptic action in pyramidal cells using whole-cell recording from rat hippocampal slices. *J. Physiol. (Lond.)* **422**, 203–225 (1990).
23. Hestrin, S., Sah, P. & Nicoll, R.A. Mechanisms generating the time course of dual component excitatory synaptic currents recorded in hippocampal slices. *Neuron* **5**, 247–253 (1990).
24. Lester, R.A.J., Clements, J.D., Westbrook, G.L. & Jahr, C.E. Channel kinetics determine the time course of NMDA receptor-mediated synaptic currents. *Nature* **346**, 565–567 (1990).
25. Popescu, G., Robert, A., Howe, J.R. & Auerbach, A. Reaction mechanism determines NMDA receptor response to repetitive stimulation. *Nature* **430**, 790–793 (2004).
26. Erreger, K., Dravid, S.M., Banke, T.G., Wyllie, D.J. & Traynelis, S.F. Subunit-specific gating controls rat NR1/NR2A and NR1/NR2B NMDA channel kinetics and synaptic signaling profiles. *J. Physiol. (Lond.)* **563**, 345–352 (2005).
27. Kampa, B.M., Clements, J., Jonas, P. & Stuart, G.J. Kinetics of Mg^{2+} unblock of NMDA receptors: implications for spike-timing dependent synaptic plasticity. *J. Physiol. (Lond.)* **556**, 337–345 (2004).
28. Sabatini, B.L. & Svoboda, K. Analysis of calcium channels in single spines using optical fluctuation analysis. *Nature* **408**, 589–593 (2000).
29. Yasuda, R., Sabatini, B.L. & Svoboda, K. Plasticity of calcium channels in dendritic spines. *Nat. Neurosci.* **6**, 948–955 (2003).
30. Naraghi, M. & Neher, E. Linearized buffered Ca^{2+} diffusion in microdomains and its implications for calculation of $[Ca^{2+}]$ at the mouth of a calcium channel. *J. Neurosci.* **17**, 6961–6973 (1997).
31. Xia, X-M. *et al.* Mechanism of calcium gating in small-conductance calcium-activated potassium channels. *Nature* **395**, 503–507 (1998).
32. Hirschberg, B., Maylie, J., Adelman, J.P. & Marrion, N.V. Gating of recombinant small conductance Ca-activated K^+ channels by calcium. *J. Gen. Physiol.* **111**, 565–581 (1998).
33. Hirschberg, B., Maylie, J., Adelman, J.P. & Marrion, N.V. Gating properties of single SK channels in hippocampal CA1 pyramidal neurons. *Biophys. J.* **77**, 1905–1913 (1999).
34. Marrion, N.V. & Tavalin, S.J. Selective activation of Ca^{2+}-activated K^+ channels by co-localized Ca^{2+} channels in hippocampal neurons. *Nature* **395**, 900–905 (1998).
35. Zorumski, C.F., Thio, L.L., Clark, G.D. & Clifford, D.B. Calcium influx through N-methyl-D-aspartate channels activates a potassium current in postnatal rat hippocampal neurons. *Neurosci. Lett.* **99**, 293–299 (1989).
36. Shah, M.M. & Haylett, D.G.K. + currents generated by NMDA receptor activation in rat hippocampal pyramidal neurons. *J. Neurophysiol.* **87**, 2983–2989 (2002).
37. Isaacson, J.S. & Murphy, G.J. Glutamate-mediated extrasynaptic inhibition: direct coupling of NMDA receptors to Ca^{2+}-activated K^+ channels. *Neuron* **31**, 1027–1034 (2001).
38. Paul, K., Keith, D.J. & Johnson, S.W. Modulation of calcium-activated potassium small conductance (SK) current in rat dopamine neurons of the ventral tegmental area. *Neurosci. Lett.* **348**, 180–184 (2003).
39. Bond, C.T. *et al.* Small conductance Ca^{2+}-activated K^+ channel knock-out mice reveal the identity of calcium-dependent afterhyperpolarization currents. *J. Neurosci.* **24**, 5301–5306 (2004).
40. Cai, X. *et al.* Unique roles of SK and Kv4.2 potassium channels in dendritic integration. *Neuron* **44**, 351–364 (2004).
41. Stocker, M., Krause, M. & Pedarzani, P. An apamin-sensitive Ca^{2+}-activated K^+ current in hippocampal pyramidal neurons. *Proc. Natl. Acad. Sci. USA* **96**, 4662–4667 (1999).
42. Goslin, K., Asmussen, H. & Banker, G. in *Culturing Nerve Cells*. 2nd edn. (eds. Goslin, K. & Banker, G.) 339–370 (MIT Press, Cambridge, Massachusetts, USA, 1998).
43. Pologruto, T.A., Sabatini, B.L. & Svoboda, K. ScanImage: flexible software for operating laser scanning microscopes. *Biomed. Eng. Online* **2**, 13 (2003).